

High Speed Nano-Optical Photodetector for Free Space Communication

Russell M. Kurtz*, Khan A. Alim, Ranjit D. Pradhan, Vladimir Esterkin, and Gajendra D. Savant
Physical Optics Corporation, Electro-Optics and Holography Division,
20600 Gramercy Blvd. Bldg. 100, Torrance, CA 90501

Rama Venkatasubramanian and Minjoo Larry Lee
RTI International, Center for Solid State Energetics
3040 Cornwallis Rd., Research Triangle Park, NC 27709

Suchismita Ghosh, Irene Calizo, and Alexander A. Balandin
Nano-Device Laboratory, Department of Electrical Engineering
University of California – Riverside, Riverside, CA 92521

ABSTRACT

An inexpensive, easily integrated, sensitive photoreceiver operating in the communications band with a 50-GHz bandwidth would revolutionize the free-space communication industry. While generation of 50-GHz carrier AM or FM signals is not difficult, its reception and heterodyning require specific, known technologies, generally based on silicon semiconductors. We present a 50 GHz photoreceiver that exceeds the capabilities of current devices. The proposed photoreceiver is based on a technology we call Nanodust. This new technology enables nano-optical photodetectors to be directly embedded in silicon matrices, or into CMOS reception/heterodyning circuits. Photoreceivers based on Nanodust technology can be designed to operate in any spectral region, the most important to date being the telecommunications band near 1.55 micrometers. Unlike current photodetectors that operate in this spectral region, Nanodust photodetectors can be directly integrated with standard CMOS and silicon-based circuitry. Nanodust technology lends itself well to normal-incidence signal reception, significantly increasing the reception area without compromising the bandwidth. Preliminary experiments have demonstrated a free-space responsivity of $50 \mu\text{A}/(\text{W}/\text{cm}^2)$, nearly an order of magnitude greater than that offered by current 50-GHz detectors. We expect to increase the Nanodust responsivity significantly in upcoming experiments.

Keywords: Nanodust, Quantum Dot Photodetector, Si/Ge Photodetector, High Speed Photodetector, Free-Space Reception, Monolithic Photoreceiver

1. INTRODUCTION

Free-space communication is important to many technologies, from military transmissions (aircraft to aircraft, satellite to ground station, etc.) to telecommunications (particularly the “last mile” from the local station to the end user). Free-space communication, like other communication technologies, can be either digital or analog. In digital systems, a signal is amplitude modulated into a string of ones and zeroes. The signal can be virtually any method of transmitting information; in standard fiber-optics based telecommunications, for example, it is an optical beam (usually a laser) operating near 1.55 μm . In analog signals, on the other hand, there is a carrier (which limits the maximum data rate) and a modulation (the data). These signals can carry the data through either amplitude or frequency modulation. Examples of these are AM (amplitude modulated) and FM (frequency modulated) radio.

The two greatest advantages of digital communication over analog are the ability to compress large amounts of data into a signal through multiplexing of frequency- and time-domain, and the simplicity of capturing, amplifying, and resending the signal (which enables near-infinite transmission lengths). The two greatest advantages of analog communication are ease of signal creation/decoding, and intrinsically high data density (an analog signal with a carrier frequency of 100 kHz and modulation rate of 44 kHz contains as much data as a typical digital system operating at 1.5 Mbps (the speed of a

* Corresponding author: rkurtz@poc.com, phone (310) 320-3088, fax (413) 208-7269

Copyright © 2007 Society of Photo-Optical Instrumentation Engineers (SPIE). This paper was published in *Micro (MEMS) and Nanotechnologies for Defense and Security* (Proc. SPIE, Vol. 6556) and is made available as an electronic reprint with permission of SPIE. One print or electronic copy may be made for personal use only. Systematic or multiple reproduction, distribution to multiple locations via electronic or other means, duplication of any material in this paper for a fee or for commercial purposes, or modification of the content of the paper are prohibited.

dedicated T-1 data line, or 1% the speed of an OC-3 digital optical fiber system). Increasing the carrier frequency to 50 GHz enables the equivalent data rate of an analog communication to be more than 10 times the speed of an OC-192, the fastest standard digital communication system currently available.

2. BACKGROUND AND THEORY

2.1. Basis of Free-Space Communication

Free-space communication is based on simple radio transmission. When you listen to the radio in your car or, watch TV received through an antenna or satellite dish, you are using free-space communication. Like radio and TV signals, any free-space communication signal must be line-of-sight; there must be a direct line from the broadcasting antenna to the receiver. This is a particular problem for “last mile” systems, but not for aircraft-to-aircraft signals or between a satellite and the ground. Purely ground-based systems can be affected by terrain (Fig. 1). If there is a direct line between the broadcast location and the receiver, not blocked by anything that is opaque at the broadcast wavelength, reception is good. Opaque objects can completely block the broadcast, and reflective objects can cause the same signal to be received from two directions at slightly different times (multipath interference), reducing the accuracy of the modulated data.

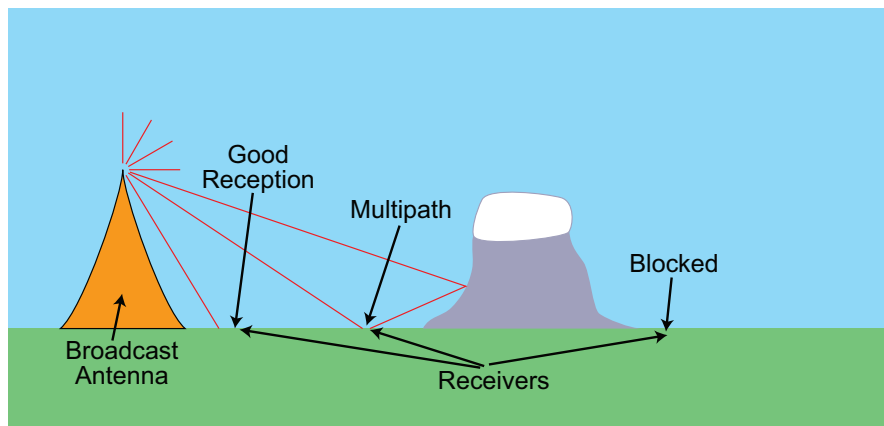


Fig. 1. Free-space communication can be affected by local geography.

Thus, typical uses of free-space communication for critical data transmission involve aircraft and satellites, which avoid interference by buildings, mountains, etc. These uses frequently require transmission over large distances without amplification, especially when communicating between satellites and ground stations. Over such distances, beam divergence is a major source of loss. Indeed, for long-range free-space communication, beam divergence is the major factor limiting the capability of receiving the signal. Since divergence affects the *intensity* of the beam, rather than its *power*, the responsivity of a free-space communications system must be specified in signal per unit intensity. In other words, the proper units for free-space responsivity would be $A/(W/cm^2)$ rather than A/W .

2.2. Free-Space Limitations

Any communications method has specific limitations. In the case of free-space, we have listed some of them in Sec. 2.1. There can be multipath interference, the signal can be blocked, and the signal divergence limits the intensity. In addition, the signal can be reduced by atmospheric extinction (absorption and scattering), and it can be affected by atmospheric turbulence. Radiation at 50 GHz, as described in Sec. 1, is attenuated at a rate of 0.1 dB/km when the air is clear and up to 0.4 dB/km in cloudy or rainy conditions¹. Turbulence is not a major loss factor at this frequency. Divergence, however, is. If the broadcast antenna is 50 cm in diameter, divergence causes a loss of 36 dB/km, far more than any other loss. A simple solution to the divergence loss is to change the carrier beam wavelength. For example, a laser whose wavelength is 1.55 μm (typical for a telecommunications laser), expanded to 50 cm diameter, has a divergence loss of only 0.12 dB/km, less than the expected loss due to atmospheric extinction (total loss for this wavelength is expected to be ~ 1 dB/km under clear conditions, up to 16 dB/km for rainy and foggy weather). This laser can then be modulated at 50 GHz, and the 50 GHz modulation signal can itself be modulated with the analog data. In effect, 50 GHz is then the intermediate frequency in a reverse superheterodyne communication broadcast system. High-

quality telecommunications lasers and 50 GHz modulators for these wavelengths are commercially available and relatively inexpensive. Unfortunately, there are few 50 GHz detectors available, and these are generally made from silicon or SiGe. Neither of these detectors is useable at 1.55 μm . InGaAs detectors are available at this wavelength, but tend to be expensive, especially at these high frequencies. In addition, we expect the signals to be weak after their long free-space travel, and the lowest-noise detection system will be one in which the photodetector is monolithically integrated with the amplifier. Silicon- and SiGe-based amplifiers provide the lowest noise and fastest response at the lowest price, so the ideal free-space detector will be compatible with silicon processing.

2.3. Nanodust

The solution we are developing is called Nanodust. It is a silicon/germanium technology closely related to quantum dots (QDs). One example of the difference between Nanodust and QDs is the exact spectrum of responsivity. QD photodetectors exhibit a large number of narrow responsivity bands (Fig. 2a), with spectral width dependent on interdot distance and spectral spacing dependent on dot size. The absorption bands are close, so only very narrow signals could pass between them. Nanodust photodetectors, on the other hand, have a continuous response (Fig. 2b), ensuring that the entire spectrum of the signal is collected, rather than the sampled spectrum of quantum dots. This is particularly important in FM analog signals.

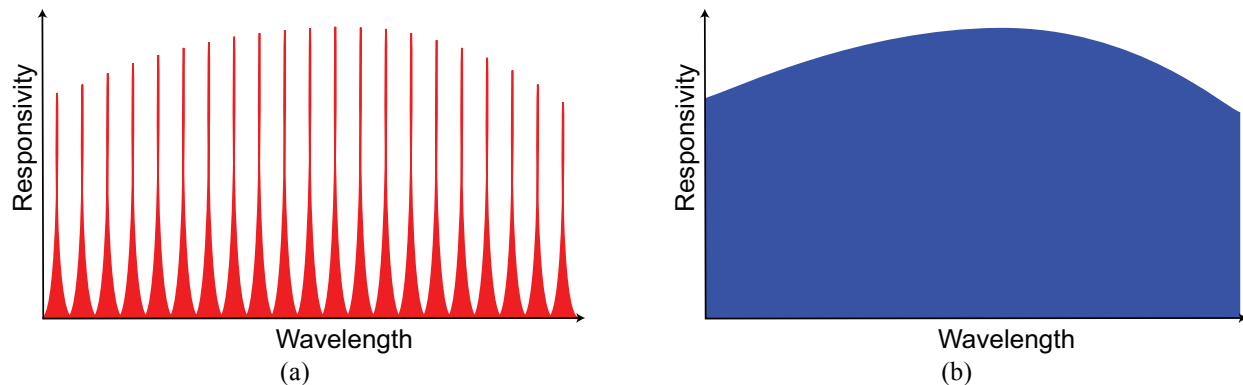


Fig. 2. Quantum dot photodetectors sample the spectrum of a signal (a) while Nanodust photodetectors collect the entire spectrum (b).

Si/Ge Nanodust has shown significant photoresponsivity at wavelengths as long as 1.6 μm , and is easily grown with standard Si techniques. Nanodust has two important characteristics in common with QDs: its photoresponse is insensitive to polarization and it can be designed to operate in normal-incidence mode, which enables a much larger detector area than the traditional side-incidence mode. Nanodust is grown in layers ~ 100 nm thick. More layers result in greater responsivity but a slower detector.

3. EXPERIMENT

Several wafers of Nanodust were fabricated at RTI. The wafers had various Ge:Si ratios and each had a different number of Nanodust layers. They were fabricated as shown in Fig. 3, a P-I-N structure with the top layer n-doped Si, the Nanodust layers as the intrinsic portion, grown on a p-doped Si substrate.

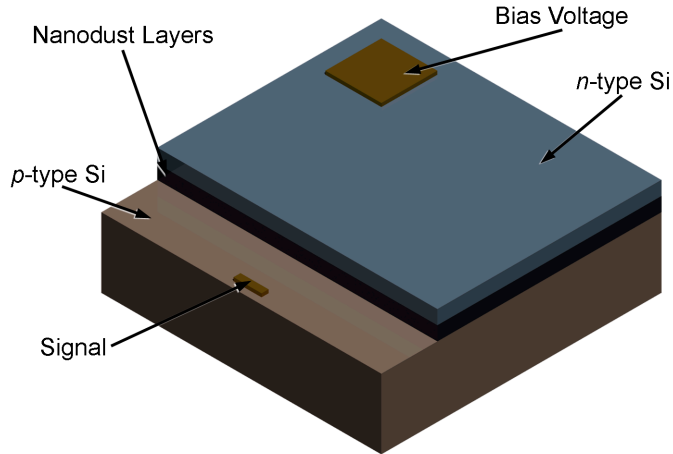


Fig. 3. Nanodust is grown as the “i” portion of a Si pin photodiode.

3.1. Material Characterization

3.1.1. Current-Voltage (I-V) Measurements

The Nanodust photodiodes were measured in both forward and reverse bias conditions, with voltage applied from the Signal pad to the Bias Voltage pad (Fig. 3). The substrate was isolated from the measurement device by electrical tape, so the capacitance and nonzero conductance of this contact may have affected the results. One photodiode I-V curve, together with the photodiode equivalent circuit, is shown in Fig. 4. This curve indicates a turn-on voltage of $V_D \sim 2.7$ V and parallel resistance $R_D \sim 12.5$ k Ω , both the worst results of this batch of 10-layer Nanodust diodes. The devices fabricated from this wafer had parallel resistances between 1 M Ω and 12.5 k Ω , and turn-on voltages from 2.4 V to 2.7 V.

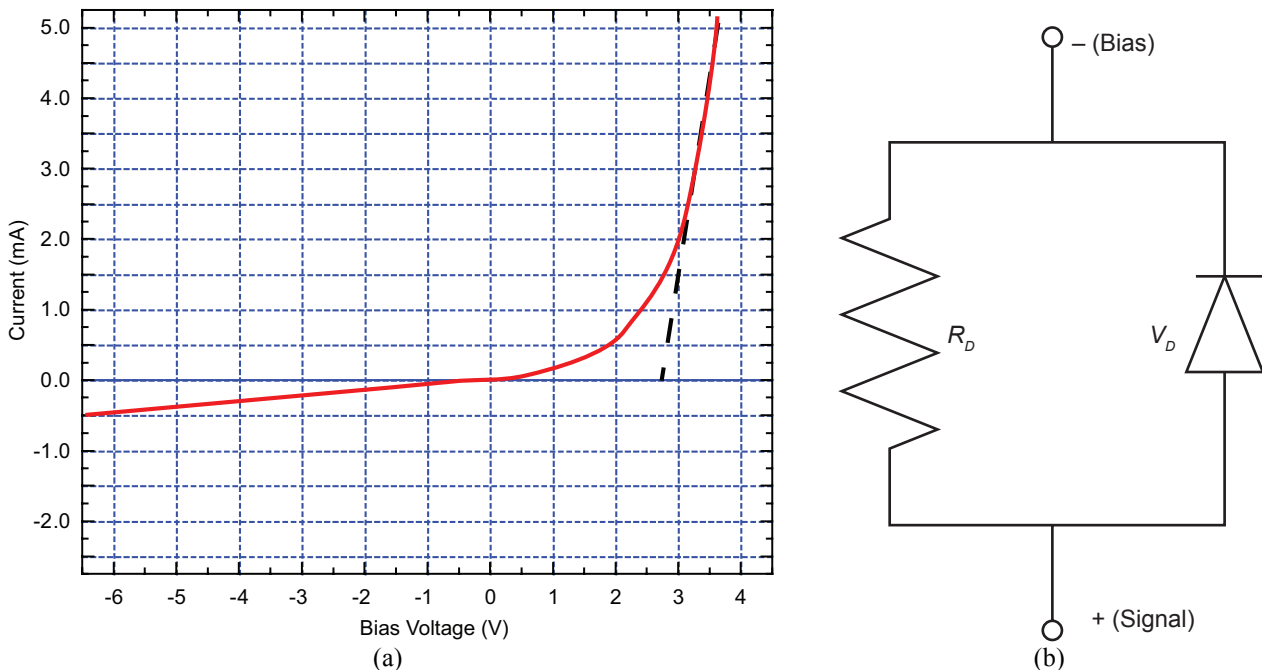


Fig. 4. The I-V characteristics of one Nanodust photodiode (a) and its equivalent circuit (b) with $R_d = 12.5$ k Ω and $V_D = 2.7$ V.

3.1.2. Capacitance-Voltage (C-V) Measurements

The capacitance of several Nanodust photodetectors was measured as a function of bias voltage and frequency. At high frequencies ($\nu > 1$ MHz), as predicted by Schottky theory, there is little variation with voltage as long as it is reverse biased. At lower frequencies the capacitance showed peaks in its C-V relationship. The peak capacitance, which occurred at reverse bias values near V_D , the forward turn-on voltage, was more than three times as large at low frequencies as at high frequencies (Fig. 5a). As the reverse bias increases to its saturation value (~ 3 V in Fig. 5b) the depletion region increases, increasing the capacitance to its saturation value (~ 10.5 pF in Fig. 5b). At lower frequencies this relationship is nonlinear, resulting in capacitance peaks, and a higher capacitance than high frequencies.

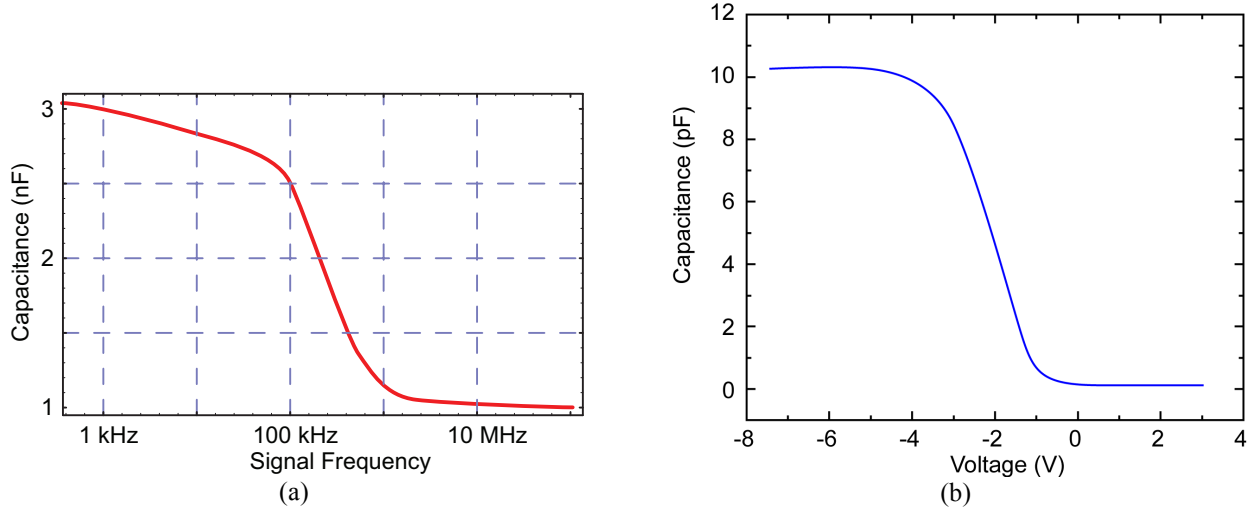


Fig. 5. Peak capacitance as a function of frequency (a) and, for high frequency, as a function of voltage (b).

Based on the capacitance measurements we expect the dielectric constant of Nanodust to be $\epsilon \approx 0.095\epsilon_0^2$.

3.1.3. Thermal Parameters

Thermal management of the integrated nanostructure-based photoreceivers is an important consideration for this novel technology, especially since their thermal conductivity is usually much smaller than that of the bulk crystals, which may complicate heat removal. We thus studied the thermal conductivity and diffusivity of the Nanodust material, using the transient Hot Disk method. The basic principle of the Hot Disk method for measuring thermal conductivity and thermal diffusivity of the material is the same as for all transient resistive heating techniques. Assuming that a cylindrical wire with the radius r_0 acts as a source of heat with constant power input per unit length, q , and is attached to the material under investigation, the temperature rise of the wire, $\Delta T = T - T_0$, can be given by the Fourier equation³

$$\Delta T \equiv T(r_0, t) - T_0 = \frac{q}{4\pi K} \ln \left[\frac{4\alpha t}{r_0^2 C} \right], \quad (1)$$

where K is the thermal conductivity, α is the thermal diffusivity, t is the time that power has been applied to the wire, and C is Euler's constant. The relationship between the thermal conductivity and thermal diffusivity is expressed as $K = \alpha C_p \rho$ (C_p is the specific heat capacity and ρ is the mass density). The results of the measurement are shown in Fig. 6. Analysis of the data shows that, at room temperature, the thermal conductivity is $K = 2.03$ W/mK, thermal diffusivity is $\alpha = 38.7$ mm²/s, and the specific heat is $C_p = 0.05$ MJ/m³K. These values include the entire structure, and are affected by the thermal boundary resistance between the nanostructured region and the Si layers. Fig. 6 shows the transient temperature in both the Nanodust material and a reference Si wafer whose parameters are $K = 148.7$ W/mK, $\alpha = 98.1$ mm²/s, and $C_p = 1.5$ MJ/m³K (and note that the amount of heat applied to the Si wafer was 10 times greater than that applied to the Nanodust wafer).

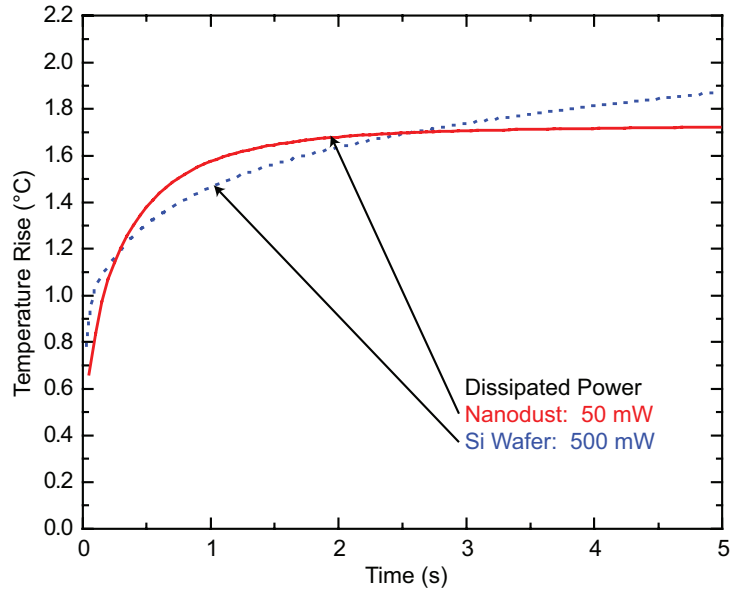


Fig. 6. Nanodust thermal conductivity and heat capacity (specific heat) were calculated from transient heating effects.

3.1.4. Stress and Dislocations

The stress and material quality can be determined by micro-Raman spectroscopy. We performed this test on two different Nanodust wafers, testing each in three locations (Fig. 7). We illuminated the wafers with the 488.0-nm line of an Ar^+ laser. Pure crystalline Si shows a Raman shift of 519 cm^{-1} and single-crystal Ge has a Raman shift of 298 cm^{-1} . In addition, a SiGe alloy has an unstrained Si-Ge bond Raman shift at 415 cm^{-1} . All these values assume measurements at room temperature. The Si-Si bond Raman shift, as expected, is the strongest in these Nanodust wafers, which are composed mainly of Si. Its location exactly on the 519 cm^{-1} single crystal Si location indicates that there is very little stress in the p- and n-type Si of these wafers. The appearance of the Ge-Ge bond Raman shift exactly at 298 cm^{-1} also indicates that there is virtually no stress in the Ge regions. The relatively strong Si-Ge bond Raman shift also occurs at its predicted value, demonstrating that the interface layers between Si and Ge are of high quality and have been grown with few dislocations.

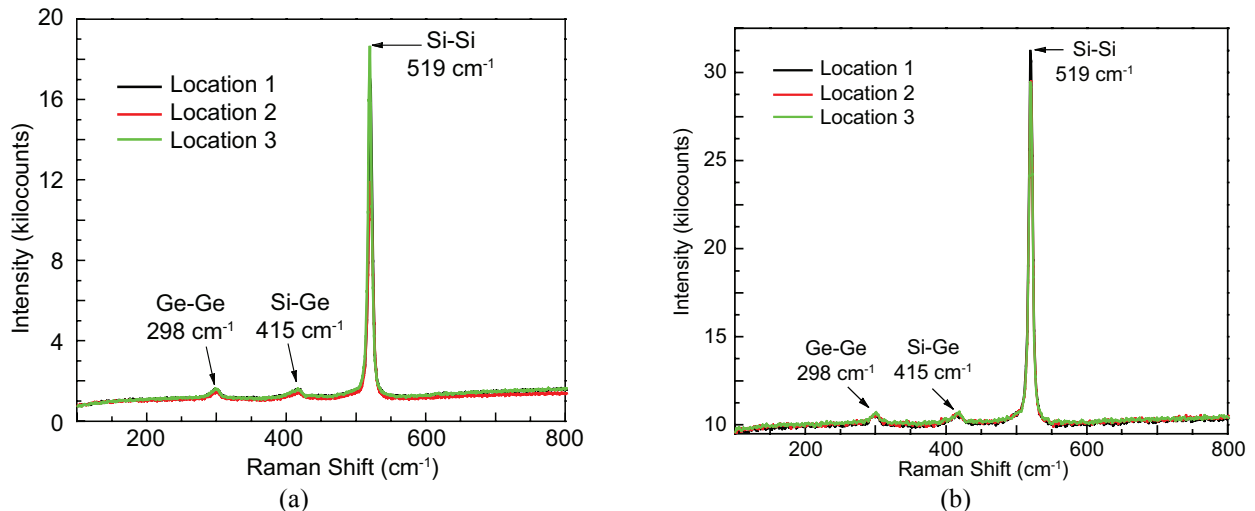


Fig. 7. Raman shifts of Si and Ge crystalline bonds show no discernable stress, while the Si-Ge bond Raman shift shows no dislocations.

3.1.5. Photoresponse

Nanodust detectors with different numbers of layers were tested for their responsivity. Each photodetector was 4 mm wide and 5 mm long (0.2 cm² area). The responsivity was measured at wavelengths from 1.47 μm to 1.60 μm and found to vary little over this region. There was a significant variation with bias voltage, however. As shown in Fig. 4, there is a significant amount of dark current, in many cases exceeding the signal. This can be eliminated either by ac-coupling the output or by using both the photodetector and an equivalent, blocked detector as inputs to a differential amplifier. Our experiments indicated that, at 3 V reverse bias, the Nanodust detector responsivity was ~5.0 μA/(W/cm²) for each layer. Since each layer absorbs a small portion of the radiation, the exponential reduction of intensity is not important for typical high-speed nanodust detectors. For very large numbers n of layers, the responsivity is

$$R \approx n \left[1 - \exp(-4 \times 10^{-5} n) \right] 5.0 \frac{\mu\text{A}}{\text{W}/\text{cm}^2} \quad (2)$$

Thus, we expect a 20-layer detector to have responsivity 100 μA/(W/cm²). Our 10-layer devices had measured responsivities of 50 μA/(W/cm²).

3.1.6. Mobility

Carrier mobility is one potential limit to the bandwidth of Nanodust devices. The device cannot react in a time shorter than it takes the carrier to transition from where it is generated in the Nanodust region to the output electrode. Mobility in the doped Si, electrodes, and wires is very high so, even though the carrier may need to move several μm in these regions, the time it takes to cross the Nanodust region will limit the overall transition time. The mobility-limited bandwidth, then, is

$$\Delta\nu \approx \frac{\mu V}{d^2} = \frac{\mu V}{(nt)^2} \quad (3)$$

where μ is the carrier mobility, V is the bias voltage (measured between the Bias and Signal electrodes in Fig. 3), t is the thickness of each Nanodust layer, and $d = nt$ is the total Nanodust thickness.

We measured the Hall mobility in a range of Ge_xSi_{1-x}/Si quantum dot superlattices, with Ge fractions of 0, 0.50, and 0.73. In this experiment, the quantum dots were dome-shaped with base size ~40 nm and height ~4 nm with a density of ~3×10⁹ cm⁻², grown by molecular beam epitaxy. We compared these measurements to identical Hall mobility measurements of Nanodust material, which has somewhat greater area density and was grown by low-pressure chemical vapor deposition. Measurements varied from 228 cm²/V-s, for a five-layer structure having a carrier density of 1.76 × 10¹⁸ cm⁻², to 239 cm²/V-s with a carrier density of 7.57 × 10¹⁸ cm⁻² in a 20-layer structure. The Nanodust material also showed Hall mobility ~230 cm²/V-s. We found that the mobility was only slightly dependent on the number of layers and the carrier density. The relatively high Hall mobility measured in these materials indicates that, as in quantum dot structures, the carrier mobility of Nanodust is based on electrons in the valence band, not hopping or trapped holes. Note that carrier mobility is proportional to T^{-3/2}, which was verified in the Hall mobility measurements. In other words, the bandwidth of the Nanodust photodetector can be increased by cooling.

4. DISCUSSION

The Nanodust photodetector has two major design tradeoffs: sensitivity increases with number of layers while bandwidth decreases as the number of layers squared. For Nanodust layers whose thickness is 30 nm each, the device sensitivity is given by Eq. (2). The capacitance is

$$C(n) = 10.5 \frac{A}{n} \text{ pF} \quad (4)$$

where A is the area of the photodetector (in mm²). Assuming the photodetector output is directed to a transimpedance amplifier of gain g , whose output impedance is 50 Ω, the detector bandwidth as limited by capacitance is

$$\Delta\nu \approx \frac{1}{2.5RC} \approx 0.761 \frac{gn}{A} \text{ GHz} \quad (5)$$

with A still in mm². The responsivity is

$$R(n) \approx 0.25 nA \text{ } \mu\text{A}/(\text{W}/\text{cm}^2) \quad (6)$$

where, again, the area is in mm². For a typical high bandwidth amplifier, the gain is 1000. The responsivity and the total bandwidth (limited by both capacitance and mobility) are shown in Fig. 8 as functions of number of layers and detector

area. Note that a typical high-speed $10\ \mu\text{m} \times 100\ \mu\text{m}$ InGaAs detector with power responsivity $500\ \text{mA/W}$ has free-space responsivity $5.0\ \mu\text{A}/(\text{W}/\text{cm}^2)$, an order of magnitude lower than a 10-layer Nanodust detector.

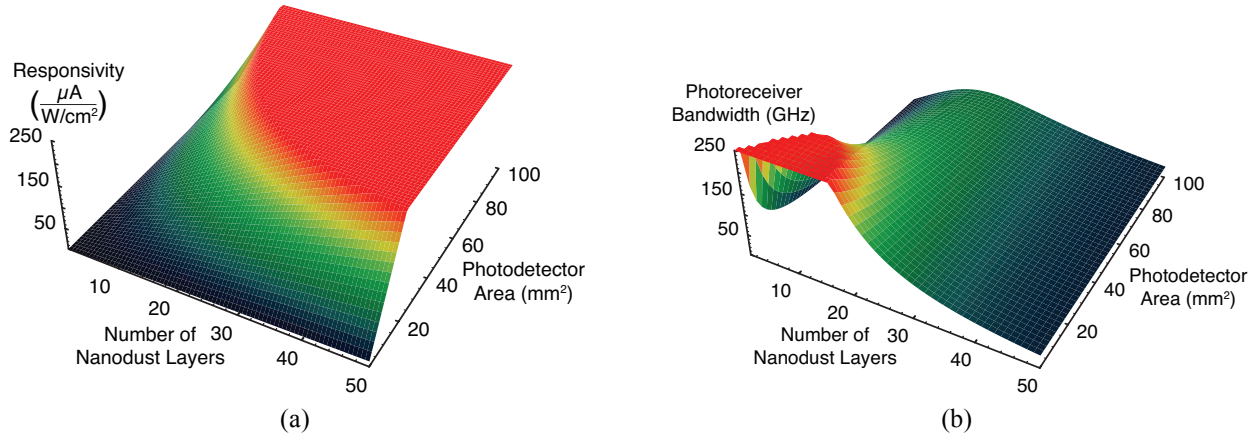


Fig. 8. While responsivity increases as a function of both number of layers and area (a), bandwidth decreases with detector area and has a peak as a function of number of layers (b).

For the specific case of a $20\ \text{mm}^2$ photodetector, such as were fabricated for this project, the tradeoff graph appears in Fig. 9. For this size, requiring bandwidth $>50\ \text{GHz}$ limits gain to $<200\ \mu\text{A}/(\text{W}/\text{cm}^2)$ – $40\times$ greater than that of existing photodetectors allowing similar bandwidth. The sensitivity can be improved by increasing either the receiver area or the number of Nanodust layers. Increasing the detector area reduces the capacitance-limited bandwidth, which is important for a small number of Nanodust layers. Increasing the number of layers, on the other hand, reduces the mobility-limited bandwidth, which is important for a large number of layers.

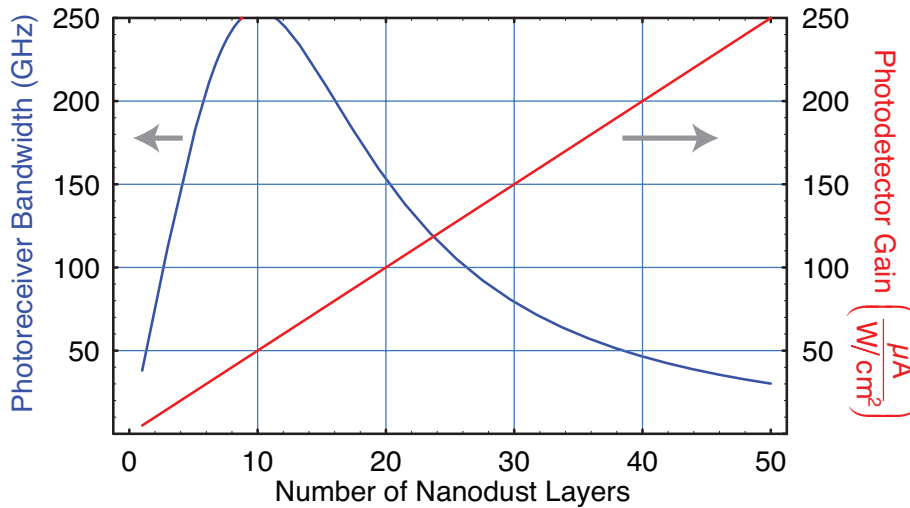


Fig. 9. Receiver bandwidth remains $>50\ \text{GHz}$ up to ~ 40 layers of Nanodust.

5. SUMMARY AND CONCLUSIONS

We have continued our study of Nanodust photoreceivers for use in the telecommunications band. These materials have been shown to work in this $1.3\text{-}1.6\ \mu\text{m}$ optical band, even though they are made with standard Si growth technologies and can be directly integrated with Si or SiGe amplifiers. Measurements of material parameters have resulted in tradeoff graphs and equations that can be used to optimize the design of a Nanodust photoreceiver.

We have shown that Nanodust photoreceivers have the capability of operation at over $250\ \text{GHz}$ bandwidth, with free-space responsivity greater than that of current telecommunications-band receivers having large bandwidth ($>10\ \text{GHz}$). A

careful design can result in a receiver with 50 GHz bandwidth, greater than current technologies, and responsivity of $200 \mu\text{A}/(\text{W}/\text{cm}^2)$, $\sim 40\times$ greater than current photoreceivers.

6. ACKNOWLEDGEMENTS

The authors gratefully acknowledge the support of the Air Force Research Laboratories, Rome, NY, under SBIR contract FA8750-05-C-0048.

7. REFERENCES

1. B.R. Bean and E.J. Dutton, *Radio Meteorology*, National Bureau of Standards Monograph 92, Colorado Springs, Colorado, 1966.
2. R.M. Kurtz, R.D. Pradhan, A.V. Parfenov, J. Holmstedt, V. Esterkin, N. Menon, T.M. Aye, K.B. Chua, and J.E. Nichter, "High Speed Nanotechnology-Based Photodetector," *Proc. SPIE Nanophotonic Materials and Systems II*, vol. 5925, 111-120, San Diego, California, 2005.
3. T.Q. Qiu and L. Tien, "Short-pulse heating on metals," *International Journal of Heat and Mass Transfer*, **35**, 719-726, 1992.